JOURNAL OF MATERIALS SCIENCE 24 (1989) 2849–2859

The role of non-cozonal twinning in the growth of fibrous silicon in strontium-modified Al–Si eutectic

M. SHAMSUZZOHA*, L. M. HOGAN
Department of Mining and Metallurgical Engineering, University of Queensland, St Lucia 4067, Australia

In fibrous growth of impurity-modified Al–Si eutectic, growth flexibility is facilitated by an extremely high twin frequency in the silicon phase. At growth rates near 300 $\mu m\,sec^{-1}$ twinning occurs on all four {1 1 1} twin planes and is restricted to first-order twins. Any pair of twins in a ⟨1 1 0⟩ zone can promote TPRE growth in a ⟨1 1 2⟩ direction and cozonal pairs of ⟨1 1 2⟩ directions can combine to give an effective ⟨1 1 0⟩ fibre axis, whereas ⟨1 1 2⟩ growth from all four twin planes results in a ⟨1 0 0⟩ fibre axis. The silicon fibres contain many twins which do not contribute in determining the fibre axis orientation at a given stage of growth. At lower growth rates the frequencies of different twin systems become unequal and fibre axis orientations can lie anywhere between ⟨1 1 0⟩ and ⟨1 0 0⟩.

1. Introduction

Impurity modification of aluminium–silicon casting alloys is achieved by trace additions of either sodium or strontium to the melt. The mechanism by which either impurity addition refines the eutectic microstructure has not yet been finally established, but recent transmission electron microscopy (TEM) studies [1–3] have shown that the sodium or strontium additions result in an enormous increase in twin density in the eutectic silicon, by comparison with the unmodified eutectic silicon.

TEM diffraction studies [2, 3] of the strontium-modified fibrous silicon have shown that the multiple twinning facilitates a zig-zag growth mechanism (Fig. 1) within each fibre. Growth at the fibre tip proceeds in two alternating ⟨1 1 2⟩ directions and, if the alternating segments are of equal size and number, the resultant fibre axis will lie parallel to either ⟨0 0 1⟩ or ⟨0 1 1⟩, as in Fig. 1. If the segments are unequal in number or volume the fibre axis can take up any crystallographic direction between these extremes [3], but at the high growth rate used in the current experiments the ⟨0 0 1⟩ and ⟨0 1 1⟩ configurations were dominant.

Growth in the ⟨1 1 2⟩ direction is typical of the twin plane re-entrant growth (TPRE) mechanism of crystal growth [4, 5] and it is assumed that each alternating segment grows by this mechanism. The alternation may be due to progressive "poisoning" of each growth front by build-up of strontium which is rejected from the solid phases and accumulates in the liquid at the growth interface. However, overgrowth of the silicon by the adjacent aluminium phase may also be important.

The crystal geometry of TPRE growth is sketched in Fig. 2a, as it appears in the flake-type growth typical of unmodified eutectic silicon [6]. The ribbon-like flakes expose {1 1 1} surfaces to the adjacent eutectic aluminium phase. Parallel {1 1 1} twins within the flake produce a stable 141° re-entrant groove at the growth interface which tends to retain silicon atoms from the melt and promotes growth in a ⟨1 1 2⟩ direction lying within the twin plane. The plates can branch through large angles by twin nucleation on the flanks, as in Figs 2b and c. The same large angle branching occurs internally in the fibres of Fig. 1 and the two possible branching angles of 70.5° and 109.5° are responsible for the two different fibre axes of Fig. 1 [3].

2. Cozonal and non-cozonal twinning

A distinctive feature of the unmodified flake eutectic silicon (Fig. 2) is that all the twin planes involved in growth and branching are cozonal. That is, in any one cluster of silicon plates (a eutectic "grain") all active twin planes contain a common ⟨0 1 1⟩ direction which would be normal to the plane of the diagram in Fig. 2. This, combined with the relatively inert {1 1 1} external surfaces, is responsible for the ribbon-like shape of the flakes. Growth of the silicon flakes can be thought of as two dimensional.

By contrast, the silicon fibres in the impurity-modified eutectic are rounded in cross-section, as in Fig. 3, and {1 1 1} facets are not prominent. In addition, the fibres tend to grow in elongated bundles, with branches appearing to grow in almost any forward direction out of a given plane containing the fibre axis. Closer observation [1, 3] suggests some

* *Present address*: College of Engineering and Mines, University of Arizona, Tucson, Arizona 85721, USA.

0022–2461/89 $03.00 + .12

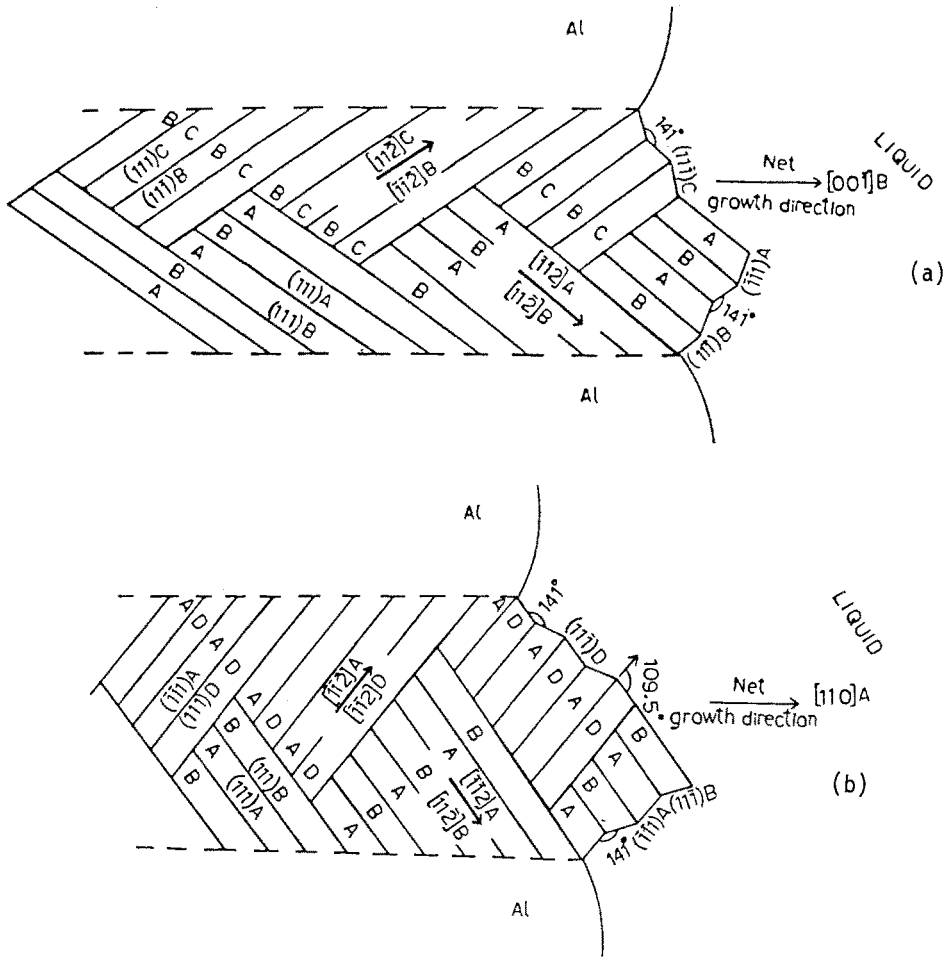

Figure 1 Growth patterns of completely modified silicon fibres in strontium-modified Al–Si eutectic. Indefinite repetition of the TPRE large angle branchings of Fig. 2 produces a zig-zag path for successive ⟨1 1 2⟩ growth segments. (a) ⟨0 0 1⟩ fibre axis with 70.5° branching; (b) ⟨1 1 0⟩ fibre axis with 109.5° branching.

limitation on branching angles, but both growth and branching are clearly three dimensional. Internal branching (Fig. 1) and external branching (Fig. 3) of the fibres both occur by the same mechanism involving twin nucleation (Figs 2b and c) and the three-dimensional growth of the fibres can only occur if non-cozonal twin planes operate. Silicon is cubic and any one silicon crystal contains {1 1 1} planes lying in four ⟨0 1 1⟩ zones. In the ribbon-like geometry sketched in Fig. 2a all active {1 1 1} twin planes belong to one of these zones, but the fibrous growth patterns of Fig. 3 would require the active twin planes to belong to more than one of the ⟨0 1 1⟩ zones, and probably

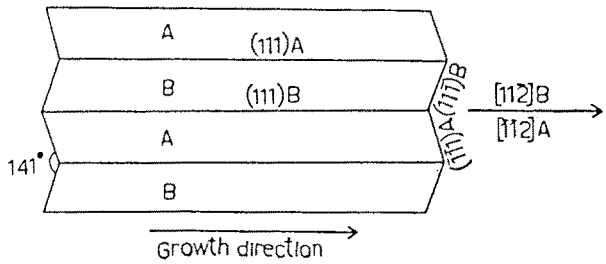

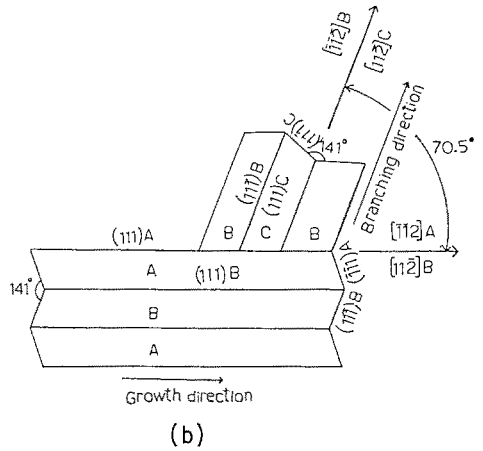

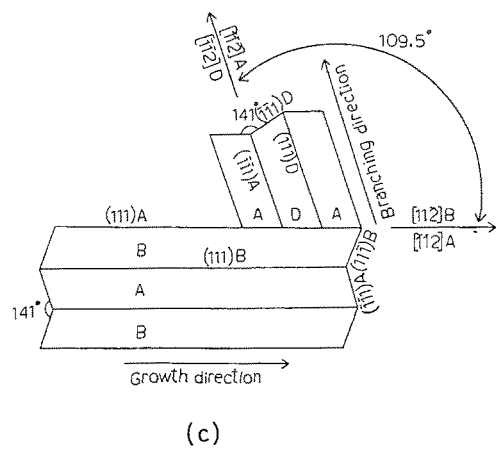

Figure 2 Schematic representation of TPRE growth patterns as observed in flake-type eutectic silicon crystals formed during unmodified growth of the aluminium–silicon eutectic. (a) in a straight silicon flake segment; (b) in large-angle 70.5° branching; (c) in large-angle 109.5° branching.

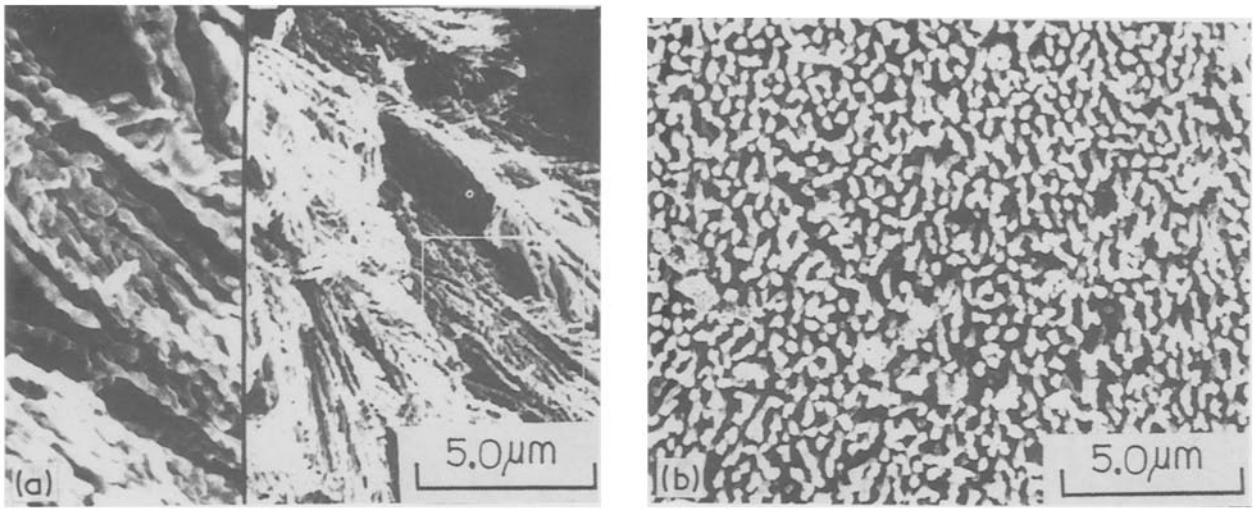

Figure 3 SEM micrographs of Al–14 wt % Si–0.18% Sr alloy directionally solidified. Growth velocity $v = 330\,\mu m\,sec^{-1}$, temperature gradient $G = 50°C\,cm^{-1}$. (a) longitudinal section, (b) transverse section. The sample was etched with 10% HF to remove aluminium phase.

to all four. Shu-Zu-Lu and Hellawell [1] were able to isolate from sodium-modified eutectic a single bundle of fibres and demonstrate that four separate active twin systems were present in the fibre.

Despite this evidence of non-cozonal twinning, the zig-zag growth mechanisms sketched in Fig. 1 were observed using diffraction techniques which detected only cozonal twins, i.e. the electron beam was aligned parallel to a single $\langle 0\,1\,1\rangle$ axis in each fibre examined. The specimen is tilted to align different $\langle 0\,1\,1\rangle$ axes in the same fibre with the beam showed that non-cozonal twinning was present [3] but, for any one point on a fibre, only one of the $\langle 0\,1\,1\rangle$ zones revealed the growth pattern of Fig. 1.

Thus, although the basic mechanism of fibrous growth is adequately described by two-dimensional diagrams such as those in Fig. 1, the detailed growth geometry is more complex. A modified diffraction technique was applied to further investigate the presence and nature of non-cozonal twinning in the silicon fibres.

3. Experimental procedure

Al–Si alloys containing 14 wt % Si and 0.18% Sr were vacuum cast from aluminium and silicon each of 99.999% purity and an Al–5 wt % Sr master alloy of 99.9% purity. The cast billets were swaged to 5 mm diameter rods then remelted and unidirectionally solidified at a rate of $330\,\mu m\,sec^{-1}$. This high rate was chosen because previous TEM studies on alloys of the same composition had shown [3] that a progressive change in the morphology of the eutectic silicon phase from partially modified to a fully modified fibre occurs as growth velocity is increased from 5 to $330\,\mu m\,sec^{-1}$. At $300\,\mu m\,sec^{-1}$ the flake silicon morphology was almost completely absent. The thermal gradient at the solid–liquid interface was determined by prior calibration of the furnace apparatus. Longitudinal and transverse specimens taken from near the centre of the solidified specimens were used for scanning electron microscopy (SEM) and thin film preparation. The thin films were prepared as described elsewhere [6] by electropolishing followed by ion beam thinning.

The thin films so prepared were examined in a Philips EM-400T electron microscope which was equipped with the facilities of convergent beam electron diffraction (CBED) techniques. Cozonal and non-cozonal twin traces in the fibrous silicon were detected when the specimen was aligned with various $\langle 0\,1\,1\rangle$ in the silicon parallel to the electron beam. Transformations between the [0 1 1] zone axes were achieved by the use of CBED Kikuchi line patterns. Appropriate Kikuchi paths connecting the zone axes were followed with the aid of the goniometer tilt in the microscope. The combination of a convergent incident beam of probe diameter < 100 nm [7] and a reduced diffraction volume, meant well-defined Kikuchi lines were obtained only for the silicon phase of the eutectic.

4. Results

After locating a silicon fibre segment in the microscope beam the goniometer tilt was used to move successively between four $\langle 0\,1\,1\rangle$ zone axes, following the Kikuchi path as in Fig. 4. Figs 5a, d, g and l show bright field micrographs from a single fibre taken at or near each of the four zone axes. The corresponding Kikuchi line patterns are given in Figs 5b, e, h and m and indexed in Figs 5c, f j and o; owing to limitations of specimen rotation, appropriate 1 1 1 Kikuchi paths leading to $\langle 0\,1\,1\rangle$ and $\langle 0\,1\,\bar{1}\rangle$ poles could not be followed up to the exact [0 1 1] and [0 1 $\bar{1}$] zone axes. Consequently, the observed Kikuchi line patterns (Figs 5h and m) for these two zone axes do not exhibit characteristics of ideal $\langle 0\,1\,1\rangle$ Kikuchi poles. Nonetheless, diffraction patterns (Figs 5i and n) of the silicon fibre at these positions of Kikuchi line patterns provided necessary crystallographic information of twins in the fibre. Each bright field micrograph exhibits two intersecting sets of cozonal twin traces.

4.1. Stereographic projection

In silicon, with four $\{1\,1\,1\}$ twin planes, the possible number of twin planes after each twinning operation is $3n + 2$, where n is the number of initial orientations [8]. Thus first-order twinning produces five possible

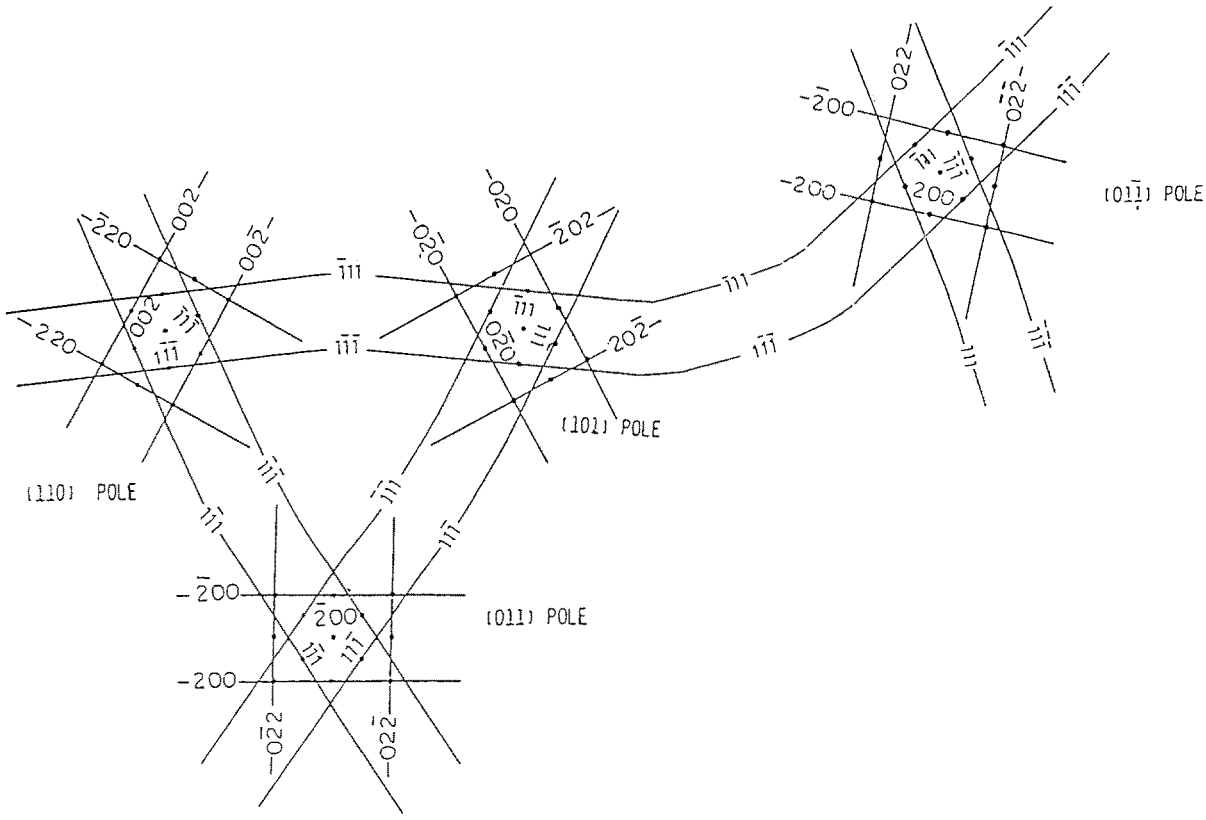

Figure 4 Schematic Kikuchi map for a fcc crystal showing four ⟨1 1 0⟩ zone axes connected by 1 1 1 Kikuchi lines.

crystal orientations and second-order twinning would increase the number of possible different orientations to 17. If second-order twinning occurs diagrammatic analysis of the twin distribution in a silicon fibre would be scarcely feasible. However, it was found possible to plot all the orientations represented in Fig. 5 on the 0 0 1 stereographic projection of Fig. 6a, in which M represents a "matrix" orientation of the silicon which contains all the observed {1 1 1} twin planes. It would appear that second-order twinning was absent or infrequent and it becomes possible to discuss the growth behaviour of the fibre by reference to the single matrix crystal. The matrix crystal poles are plotted alone in Fig. 6b. In both diagrams the twin plane traces are drawn in and assigned the indices (1 1 1), ($\bar{1}$ 1 1), ($\bar{1}$ $\bar{1}$ 1) and (1 $\bar{1}$ 1) with reference to the matrix crystal. In Fig. 6a the twins formed on these matrix planes are represented as crystals A, B, C and D in the same sequence. 1 1 2 and 1 1 0 poles are also plotted for the matrix and for the four twin orientations. The twin planes and the directions of the twin traces in Fig. 5 are then identified in Table I, for each of the four ⟨1 1 0⟩ zone axes identified in Fig. 5.

In the TEM observations of Fig. 5 only four of the six possible ⟨0 1 1⟩ zone axes were accessible, due to limitations of specimen rotation. Each zone axis revealed two ⟨1 1 2⟩ directions, so that only eight of the twelve possible ⟨1 1 2⟩ directions could be observed. Trials on a number of thin films were necessary before this total could be reached. Nonetheless, all four twin orientations A, B, C and D appear in Table I, indicating that twinning occurred on all available twin planes of the matrix crystal.

In Fig. 6b traces of the six {1 1 0} planes are drawn into the centre of the diagram, each connecting pairs of cozonal ⟨1 1 2⟩ directions which could combine to produce the zig-zag growth patterns of Fig. 1b. The actual growth axis for this fibre was identified as [$\bar{1}$ 1 0] with respect to the matrix, as marked in Fig. 6. The geometry of the growth pattern can be read from Fig. 6 and is represented in Fig. 7 with reference to the matrix crystal.

The (1 1 0) trace in Fig. 6b passes through ⟨0 0 1⟩ and connects the poles $\bar{1}$ 1 2 and 1 $\bar{1}$ 2 of the matrix. These lie in the twin planes (1 $\bar{1}$ 1) and ($\bar{1}$ 1 1) which intersect along [1 1 0] in Fig. 7. The observed fibre axis

TABLE I Growth characteristics of twins present in the silicon fibre of fig. 5

Micrograph number	Zone axis	Twin plane	Direction of twin traces	
5a, b, c	[1 0 1] M, B, C	($\bar{1}$ 1 1) M, B	[$\bar{1}$ $\bar{2}$ 1] M	[1 2 $\bar{1}$] B
		(1 1 $\bar{1}$) M, C	[1 $\bar{2}$ $\bar{1}$] M	[$\bar{1}$ 2 1] C
*5d, e, f	[1 1 0] M, B, D	(1 $\bar{1}$ $\bar{1}$) M, B	[$\bar{1}$ 1 $\bar{2}$] M	[1 $\bar{1}$ 2] B
		(1 $\bar{1}$ 1) M, D	[$\bar{1}$ 1 2] M	[1 $\bar{1}$ $\bar{2}$] D
5g, h, i, j, k	[0 1 1] M, C, D	(1 1 $\bar{1}$) M, C	[$\bar{2}$ 1 $\bar{1}$] M,	[2 $\bar{1}$ 1] C
		(1 $\bar{1}$ 1) M, D	[$\bar{2}$ $\bar{1}$ 1] M,	[2 1 $\bar{1}$] D
5l, m, n, o, p	[0 1 $\bar{1}$] M, A, B	(1 1 1) M, A	[2 1 1] M,	[2 $\bar{1}$ $\bar{1}$] A
		(1 $\bar{1}$ $\bar{1}$) M, B	[$\bar{2}$ $\bar{1}$ $\bar{1}$] M,	[2 1 1] B

*Only this twin system contributed to the growth of the fibre, following the growth pattern of Fig. 1(b).

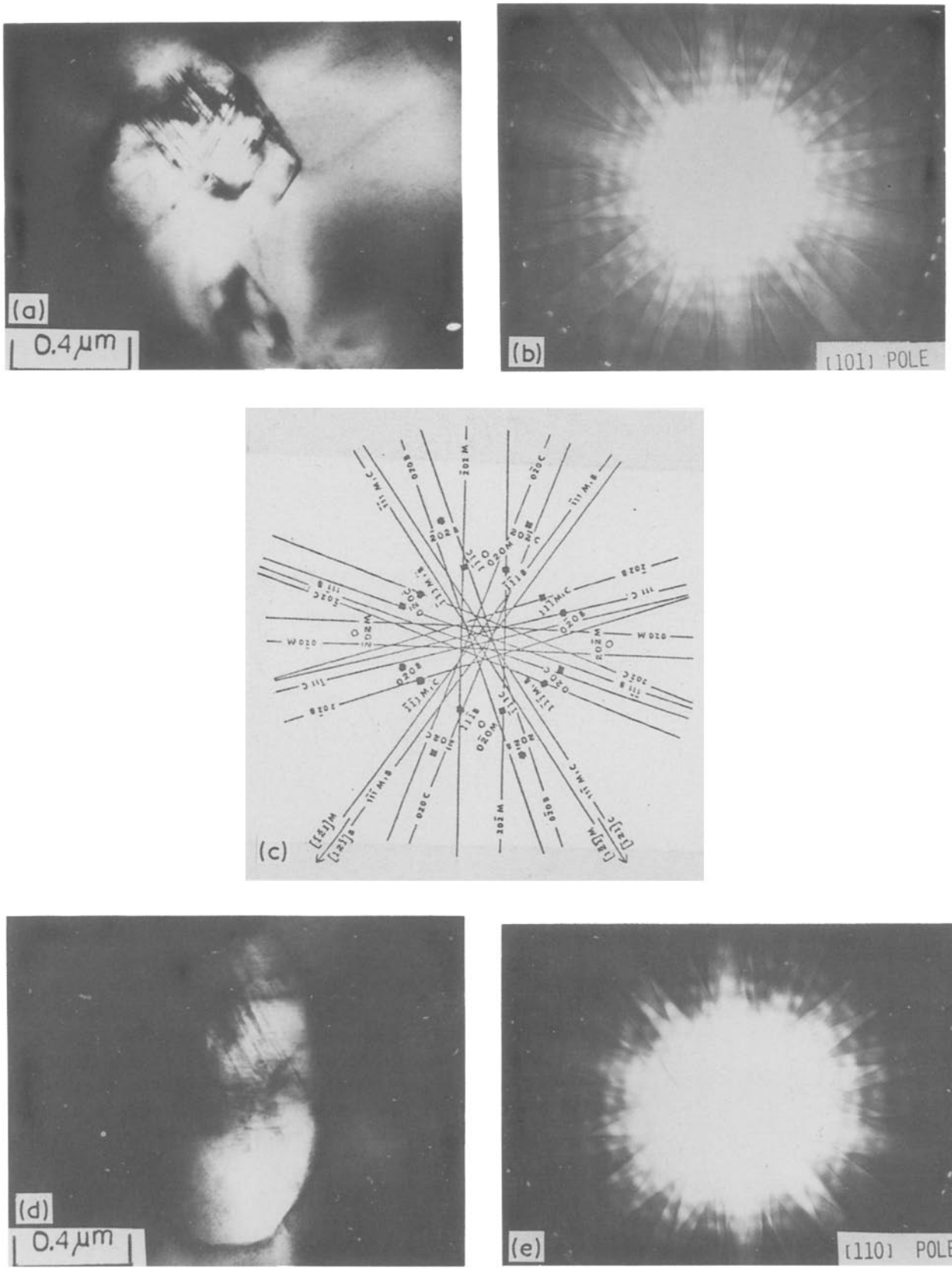

Figure 5 TEM micrographs illustrating the presence of twinning in all four {1 1 1} planes in a strontium-modified fibre. Al–14% Si–0.18%Sr. $v = 330\,\mu m\,sec^{-1}$, $G = 50°\,C\,cm^{-1}$ (a), (d), (g), (l): Bright field micrographs of the same fibre segment with electron beam parallel to four different ⟨1 1 0⟩ crystal orientations; (b), (e), (h), (m): Kikuchi line patterns at (a), (d), (g), (l); (c), (f), (j), (o): Key to Kikuchi patterns; (i), (n): Diffraction patterns taken from the fibre segment for its [0 1 1] and [0 1 $\bar{1}$] orientations; (k), (p): Keys to diffraction patterns.

[$\bar{1}$ 1 0] lies in the [1 1 0] zone with [$\bar{1}$ 1 2] and [$\bar{1}$ 1 $\bar{2}$] and corresponds with the configuration of Fig. 1b. Fig. 6a shows that [$\bar{1}$ 1 2] and [$\bar{1}$ 1 $\bar{2}$] in the matrix correspond to [1 $\bar{1}$ $\bar{2}$] and [1 $\bar{1}$ 2] in the twin crystals D and B respectively (remembering that [$\bar{1}$ 1 $\bar{2}$] plots at 180° from [1 $\bar{1}$ 2] and would appear on the lower half of the projection sphere). These indices are listed in Table I for Figs 5d, e and f. In Fig. 1b the indexing is different but the crystals A, B and D correspond to the matrix A and twin crystals B and D.

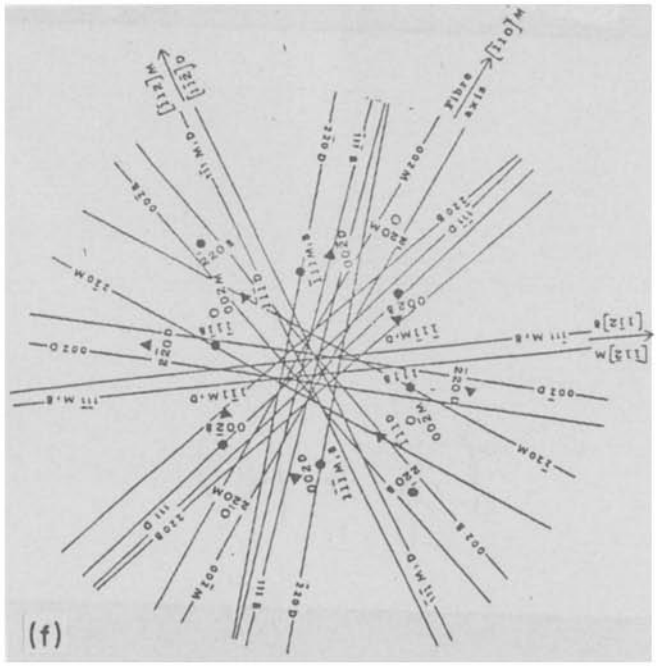

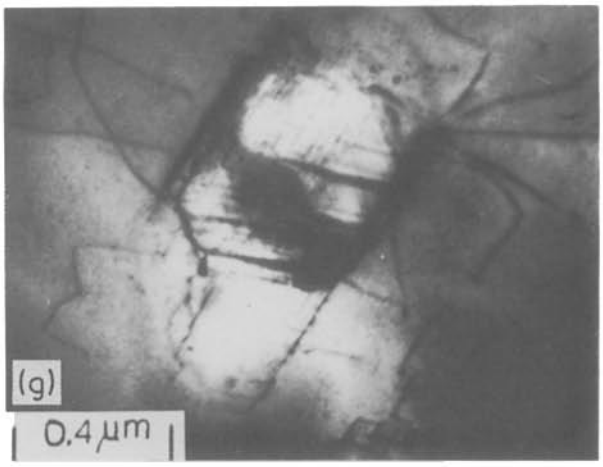

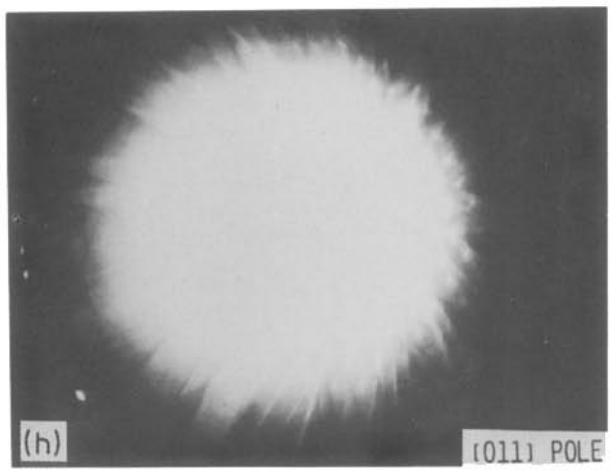

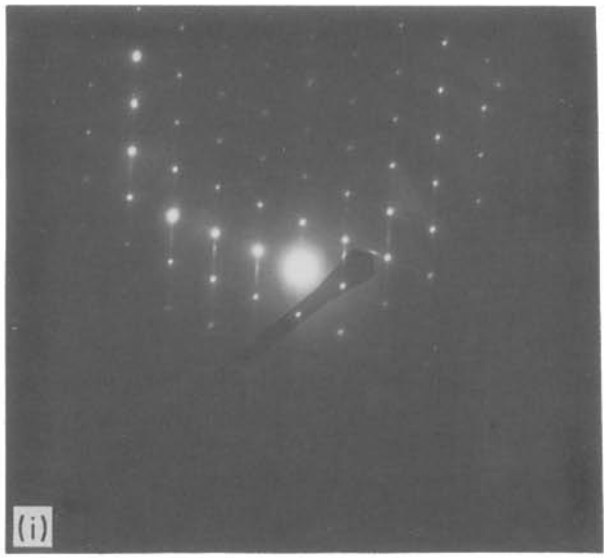

Figure 5 Continued

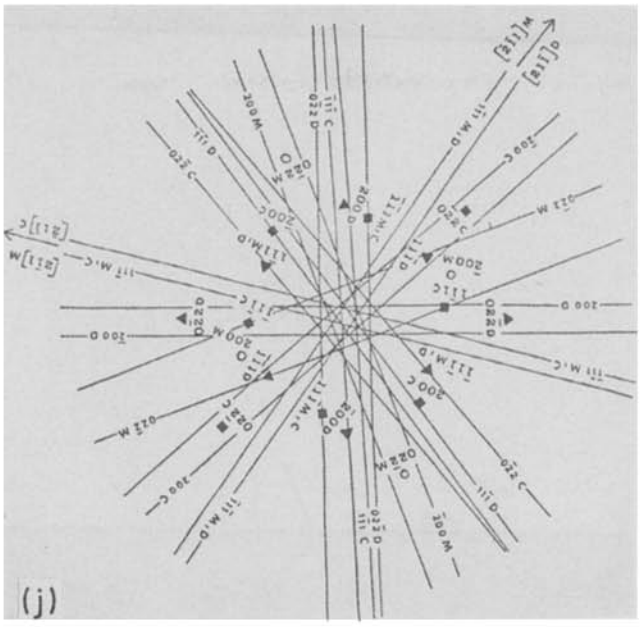

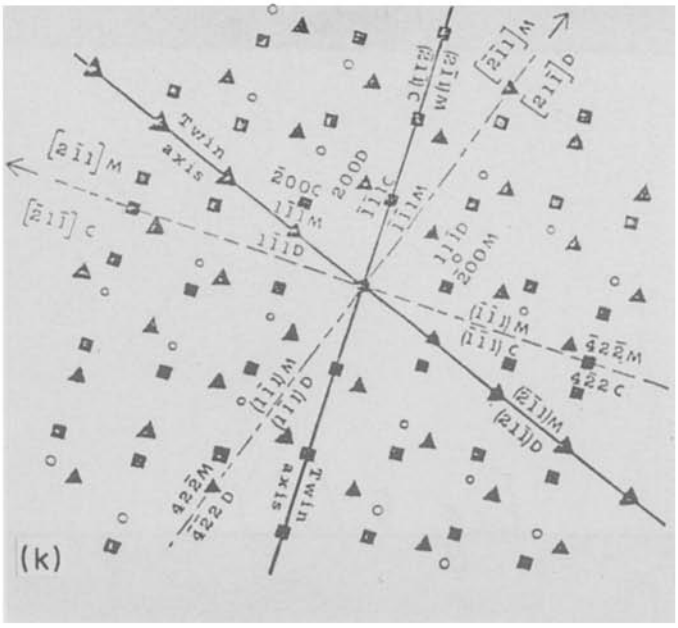

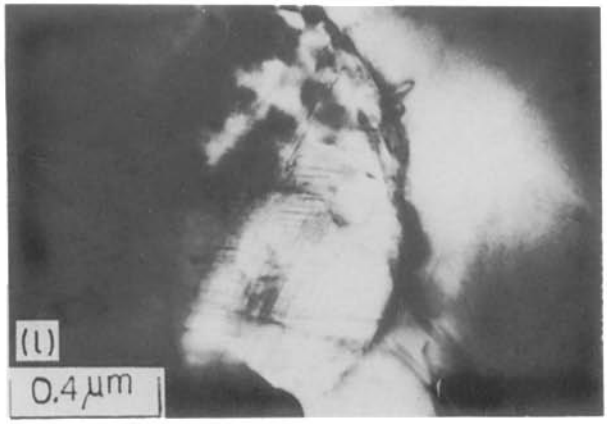

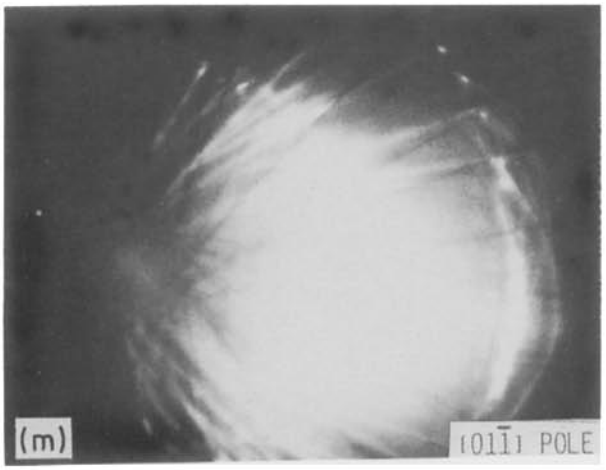

Figure 5 Continued

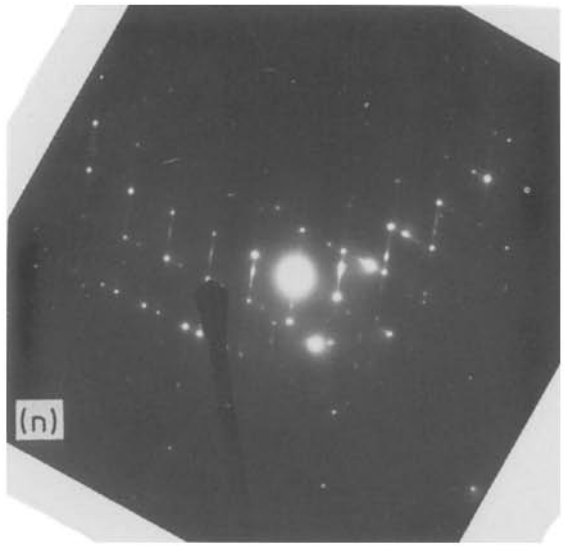

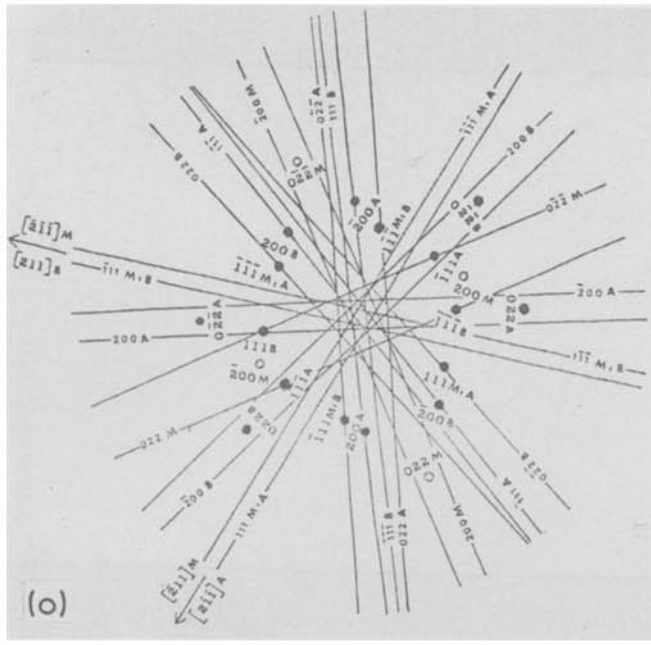

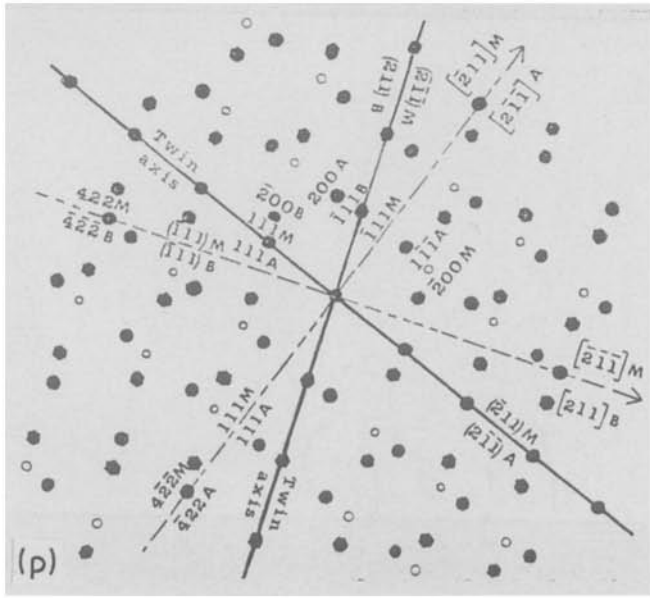

Figure 5 Continued

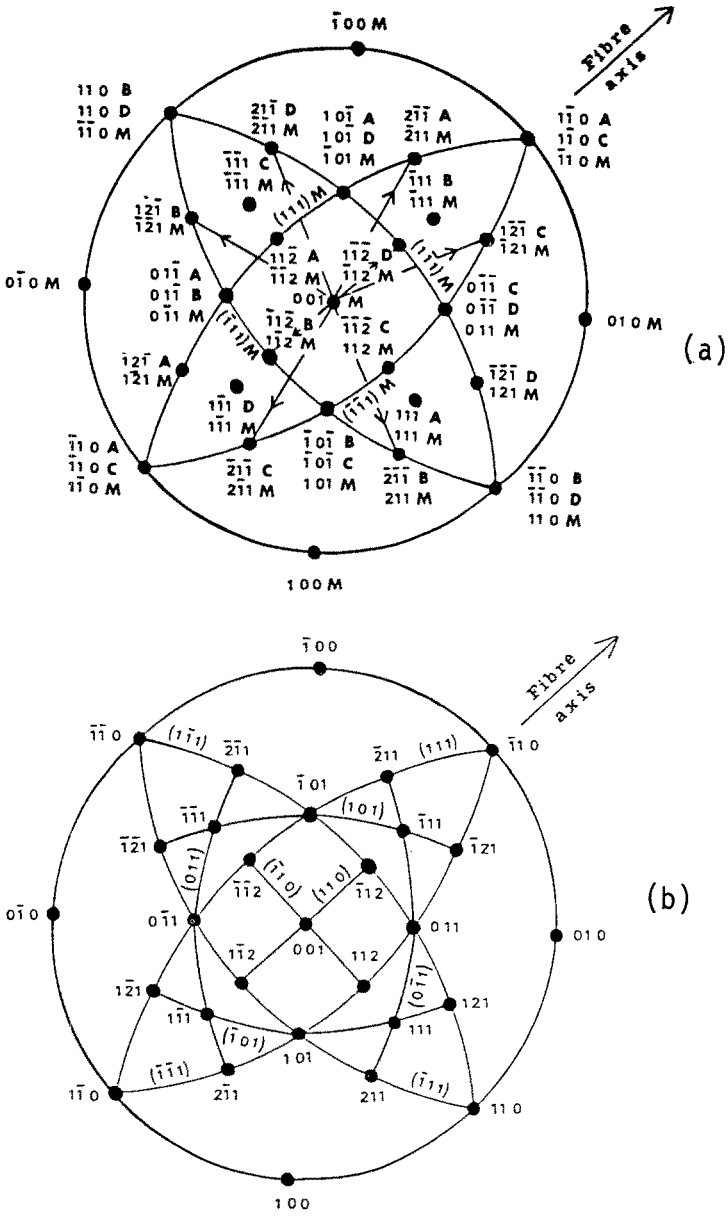

Figure 6 0 0 1 stereographic projections for silicon, showing effective ⟨1 1 0⟩ fibre axis as in Fig. 1(b). (a) {1 1 1} twin planes and 1 1 0 and 1 1 2 poles for matrix orientation M and four first-order twin orientations, A, B, C and D. (b) Poles of matrix crystal, {1 1 1} twin plane traces and traces of {1 1 0} planes connecting alternating ⟨1 1 2⟩ pairs.

Fig. 7 also shows that, if the growth directions in the two twin planes had been $[\bar{1}\,1\,2]$ and $[1\,\bar{1}\,2]$, the fibre growth direction would have been [0 0 1] as in Fig. 1a, with the 70.5° configuration of Fig. 2b. Clearly the $[\bar{1}\,1\,0]$ fibre axis was selected because it lay closest to the overall growth direction of the eutectic. However, reference to Fig. 6a shows that ⟨0 0 1⟩ growth differs from ⟨1 1 0⟩ growth in that all four {1 1 1} twin systems can operate simultaneously to produce the zig-zag growth pattern of Fig. 1a; e.g. the directions [1 1 2], $[\bar{1}\,1\,2]$, $[\bar{1}\,\bar{1}\,2]$, $[1\,\bar{1}\,2]$ are symmetrical about 0 0 1 in Fig. 6b, indicating that if the remaining two {1 1 1} planes were drawn into Fig. 7, intersecting along $[\bar{1}\,1\,0]$, they would form a pyramid with [0 0 1] as axis. The cubic crystal has fourfold symmetry about ⟨0 0 1⟩ but only twofold symmetry about ⟨1 1 0⟩. ⟨0 0 1⟩ fibre growth in conformity with this fourfold symmetry has been observed by Shu-Zu-Lu and Hellawell [1] and confirmed in the present work. Diffraction patterns taken with the beam on two mutually perpendicular ⟨1 1 0⟩ zone axes normal to the ⟨0 0 1⟩ fibre axis are identical and corresponding TEM micrographs reveal similar twin traces. In each case analysis produces the growth pattern of cozonal twins shown in Fig. 1a. The symmetry is evident in Figs 5g and i, and 5l and n although in this case ⟨0 0 1⟩ was not chosen as the fibre axis.

Table I lists the twin trace directions for the other three zone axes used for the micrographs of Fig. 5. In each case the configuration is as in Fig. 7 and the twin pairs are capable of permitting growth in either a [1 0 0] or [1 1 0] direction. It is to be expected that the missing $[\bar{1}\,0\,1]$ and $[\bar{1}\,1\,0]$ zone axes would have revealed similar twin pairs, since all four twin orientations appear in Table I. Thus potential growth directions, for which the necessary twin pairs are present in the growing crystal, comprise twelve ⟨1 1 0⟩ directions and six ⟨1 0 0⟩ directions, since growth is possible in either sense for each direction. To this must be added 24 ⟨1 1 2⟩ directions, making a total of 42 directions in which growth could take place from a given segment of fibre. The directions would project fairly evenly onto the surface of a sphere and the average angle between direction vectors would be of the order 35°. Branching angles would be of this order, so that smooth adjustments to interfibre spacing to accommodate small changes in melt composition and temperature gradient would be difficult as is evident in Fig. 3

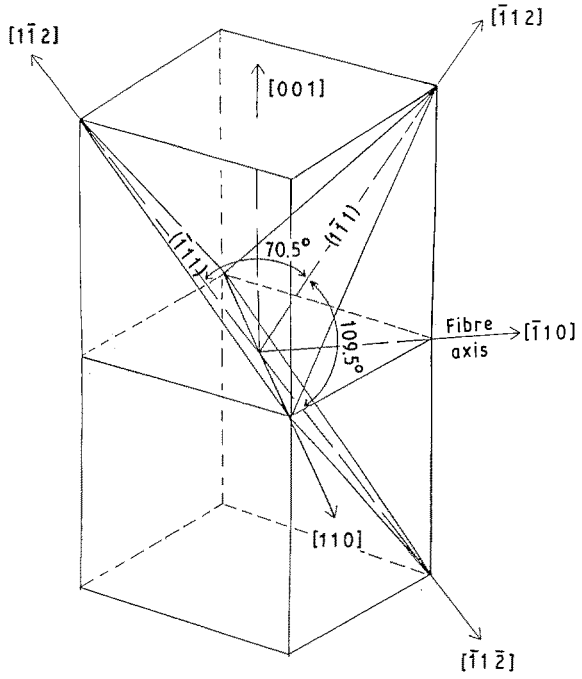

Figure 7 Effective fibre axis [1 1 0] in relation to the alternating segments growing in [1 1 2] and [1 1 2] directions (matrix orientation). The diagram shows that an effective [0 0 1] fibre axis would be equally possible if it were favoured by the overall heat extraction direction.

where the fibrous growth is quite irregular compared with that in a nonfaceted–non faceted eutectic. However, the multitude of twins permits rapid successions of direction changes which can result in somewhat smaller apparent branching angles.

It must be emphasized that these conditions apply to high growth rates of the modified eutectic exceeding about 300 μm sec^{-1}, when the twin frequency is so high that all first-order twin sites are active to an approximately equal extent. Under these conditions ⟨1 1 0⟩ and ⟨1 0 0⟩ fibre axis directions are strongly favoured. As growth rate decreases the twin frequency decreases and it would appear that the statistical spread allows a more and more pronounced unbalance between the activities of different twin sites. The observed result [3] is that, at slower rates, the silicon fibre growth can take up any crystallographic direction between ⟨1 0 0⟩ and ⟨1 1 0⟩, through ⟨1 1 2⟩. At extremely slow growth rates the strontium modified eutectic silicon tends to revert to the cozonal twinning typical of unmodified flake silicon eutectic. At the other extreme it is possible that second-order twins would appear at very high growth rates, thus again increasing the range of branching angles, but this has not been investigated.

5. Discussion

These observations show that, at a growth rate in the neighbourhood of 300 μm sec^{-1}, the silicon fibres in impurity modified eutectic can exhibit first-order twinning on all four {1 1 1} twin planes of a matrix silicon orientation, with roughly equal twin frequency on each plane at all points along the fibre. Any of these twin pairs can promote TPRE growth in a ⟨1 1 2⟩ direction within the twin plane and cozonal pairs of ⟨1 1 2⟩ directions can combine to give an effective ⟨1 1 0⟩ fibre axis by alternating TPRE growth in the zig-zag pattern of Fig. 1b. A frequent alternative is the combination of ⟨1 1 2⟩ growth from all four twin planes to produce a ⟨1 0 0⟩ fibre axis as in Fig. 1a.

The presence of this multitude of twin pairs in the fibre provides freedom for the fibre to branch in many directions in attempting to maintain a uniform interfibre spacing when local melt conditions change at the interface, but the branching angles are quite large, usually over 30°. It follows that the growth pattern, as in Fig. 3, is necessarily much more ragged than is observed in non-faceted–non-faceted fibrous eutectics, where the fibres can change growth direction through very small angles in response to changes in melt conditions.

The preference for ⟨1 1 0⟩ and ⟨1 0 0⟩ fibre axes depends on the presence of approximately equal numbers of twin events on all first-order twin sites, so that in the configurations of Fig. 1 the alternating ⟨1 1 2⟩ directions can occur with equal frequency. This appears to be a statistical effect, in that the fibre axis

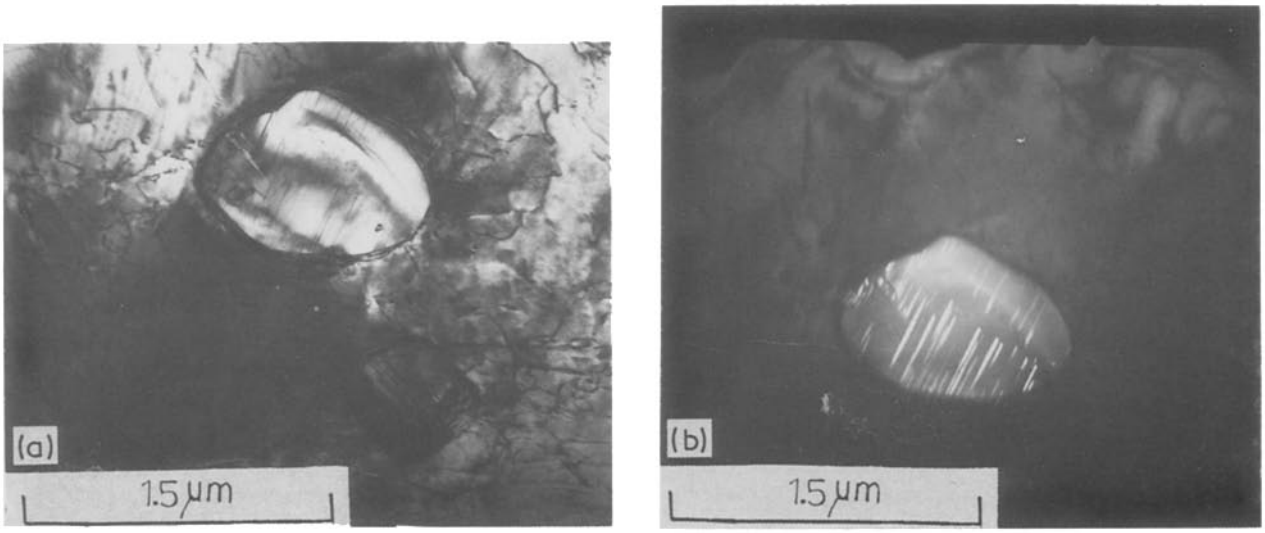

Figure 8 TEM micrographs showing {1 1 1} twinning in impurity modified silicon fibre. Al–14% Si–0.18%Sr, v = 89 μm sec^{-1}, G = 50° C cm^{-1}. (a) Transverse section, bright field micrograph, exhibiting two intersecting sets of cozonal twin traces belonging to {1 1 1} twin planes; (b) Dark field micrograph selecting one of the two twin orientations in (a).

orientations become more random at lower growth rates. As growth rate decreases the overall twinning frequency decreases and the distribution of twin events between the four {1 1 1} twin planes would become more uneven. Conversely, it might be expected that second-order twinning may appear at very high growth rates, leading again to more variable fibre axis orientations.

The distribution of the non-operative twin planes, seen as traces in Figs 5a, g and l, remains unclear. Dark field micrographs show many individual twin traces to be discontinuous, appearing as dot-dash lines with the discontinuities filled by twins of different orientation (Fig. 8). In bright field micrographs the twin traces form intersecting patterns, as in Fig. 5. It seems that twins of different orientation are present throughout the thickness of any given fibre segment. It may be that twins of different orientation exist in successive layers through the thickness of a fibre and grow laterally to interpenetrate neighbouring layers.

References

1. SHU-ZU-LU and A. HELLAWELL, *J. Cryst. Growth* **28** (1985) 171.
2. M. SHAMSUZZOHA, PhD Thesis, University of Queensland (1986).
3. M. SHAMSUZZOHA and L. M. HOGAN, *Phil. Mag.* **54** (1986) 459.
4. R. S. WAGNER, *Acta Metall.* **8** (1960) 57.
5. D. R. HAMILTON and R. G. SEIDENSTICKER, *J. Appl. Phys.* **31** (1960) 1165.
6. M. SHAMSUZZOHA and L. M. HOGAN, *J. Cryst. Growth* **76** (1986) 429.
7. J. B. WILLIAMS, *Norelco Reporter* **30** (1983), 24.
8. M. G. DAY and A. HELLAWELL, *Proc. R. Soc.* **A305** (1968) 473.

Received 1 June
and accepted 21 October 1988